Research Article | Vol. 25, No. 1 | 9 Jan 2017 | OPTICS EXPRESS 409

Optics EXPRESS

Reduction of the operating voltage of a nanoencapsulated liquid crystal display by using a half-wall structure

YOU-JIN LEE,[1,3] MINHO PARK,[1,3] DONG-MYUNG LEE,[2,*] CHANG-JAE YU,[1,2] AND JAE-HOON KIM[1,2,*]

[1]*Department of Electronic Engineering, Hanyang University, Seoul 133-791, South Korea*
[2]*Department of Information Display Engineering, Hanyang University, Seoul 133-791, South Korea*
[3]*These authors contributed equally to this work*
[*]*jhoon@hanyang.ac.kr*

Abstract: We proposed a half-wall structure in the in-plane switching (IPS) configuration of the nanoencapsulated liquid crystal (LC) display for reducing a driving voltage. The IPS electrodes were fabricated on top of the half-walls to enhance electric field strength through the whole LC layer. In addition, we demonstrated a self-masking process for the half-wall structure and the IPS electrodes without any additional mask-aligning process.

OCIS codes: (120.2040) Displays; (230.3720) Liquid-crystal devices.

References and links

1. M. Oh-e and K. Kondo, "Electro-optical characteristics and switching behavior of the in-plane switching mode," Appl. Phys. Lett. **67**(26), 3895–3897 (1995).
2. M. Oh-e, M. Yoneya, M. Ohta, and K. Kondo, "Dependence of viewing angle characteristics on pretilt angle in the in-plane switching mode," Liq. Cryst. **22**(4), 391–400 (1997).
3. S. H. Lee, S. L. Lee, and H. Y. Kim, "Electro-optic characteristics and switching principle of a nematic liquid crystal cell controlled by fringe-field switching," Appl. Phys. Lett. **73**(20), 2881–2883 (1998).
4. I. H. Yu, I. S. Song, J. Y. Lee, and S. H. Lee, "Intensifying the density of a horizontal electric field to improve light efficiency in a fringe-field switching liquid crystal display," J. Phys. D **39**(11), 2367–2372 (2006).
5. P. J. Bos and L. R. Koehler, "The pi-cell: a new, fast liquid-crystal optical switching device," Mol. Cryst. Liq. Cryst. **113**(1), 329–339 (1984).
6. Y. Yamaguchi, T. Miyashita, and T. Uchida, "Wide-viewing-angle display mode for the active-matrix LCD using bend-alignment liquid-crystal cell," in *Digest of Technical Papers of 1993 Society for Information Display International Symposium* (1993), pp. 277–280.
7. S. Yamauchi, M. Aizawa, J. F. Clerc, T. Uchida, and J. Duchen, "Homeotropic-alignment full-color LCD," in *Digest of Technical Papers of 1989 Society for Information Display International Symposium* (1989), pp. 378–381.
8. S. Ohmuro, S. Kataoka, T. Sasaki, and Y. Koike, "Development of super-high-image-quality vertical-alignment mode LCD," in *Digest of Technical Papers of 1997 Society for Information Display International Symposium* (1997), pp. 845–848.
9. A. Takeda, S. Kataoka, T. Sasaki, H. Chida, H. Tsuda, K. Ohmuro, T. Sasabayashi, Y. Koike, and K. Okamoto, "A super-high image quality multi-domain vertical alignment LCD by new rubbing-less technology," in *Digest of Technical Papers of 1998 Society for Information Display International Symposium* (1998), pp. 1077–1080.
10. K. Sueoka, H. Nakamura, and Y. Taira, "Improving the moving-image quality of TFT-LCDs," in *Digest of Technical Papers of 1997 Society for Information Display International Symposium* (1997), pp. 203–206.
11. K. H. Kim, K. Lee, S. B. Park, J. K. Song, S. N. Kim, and J. H. Souk, "Domain divided vertical alignment mode with optimized fringe field effect," in *Proceeding of The 18th International Display Research Conference Asia Display* (1998), pp. 383–386.
12. N. Yamada, S. Kohzaki, F. Funada, and K. Awane, "Axially symmetric aligned microcell (ASM) mode: electrooptical characteristics of new display mode with excellent wide viewing angle," in *Digest of Technical Papers of 1995 Society for Information Display International Symposium* (1995), pp. 575–578.
13. H. Kikuchi, M. Yokota, Y. Hisakado, H. Yang, and T. Kajiyama, "Polymer-stabilized liquid crystal blue phases," Nat. Mater. **1**(1), 64–68 (2002).
14. Y. Hisakado, H. Kikuchi, T. Nagamura, and T. Kajiyama, "Large electro-optic Kerr effect in polymer-stabilized liquid-crystalline blue phases," Adv. Mater. **17**(1), 96–98 (2004).
15. M. Kim, M. S. Kim, B. G. Kang, M.-K. Kim, S. Yoon, S. H. Lee, A. Ge, L. Rao, S. Gauza, and S.-T. Wu, "Wall-shaped electrodes for reducing the operation voltage of polymer-stabilized blue phase liquid crystal displays," J. Phys. D Appl. Phys. **43**(23), 235502 (2009).

#276274 http://dx.doi.org/10.1364/OE.25.000409
Journal © 2017 Received 24 Nov 2016; revised 29 Dec 2016; accepted 1 Jan 2017; published 6 Jan 2017

Optics EXPRESS

16. S.-G. Kang and J.-H. Kim, "Optically-isotropic nanoencapsulated liquid crystal displays based on Kerr effect," Opt. Express **21**(13), 15719–15727 (2013).
17. T. Kissel, S. Maretschek, C. Packhauser, J. Schneiders, and N. Seidel, *Microencapsulation*, S. Benita ed. (CRC, 2006), pp. 103.

1. Introduction

Liquid crystal displays (LCDs) have been extensively studied and used for a wide range of display applications including mobile phones, monitors, and televisions because of their high image qualities with low power consumption. However, LCDs have some intrinsic problems such as slow response time and narrow viewing angle characteristics. To overcome the viewing angle problem, multi-domain LC modes have been proposed such as in-plane switching (IPS) [1,2], fringe-field switching [3,4], optically-compensated bend [5,6], muti-domain vertical alignment [7–9], patterned vertical alignment [10,11], and axially symmetric aligned microcell [12], polymer-stabilized blue phase LC modes [13–15]. The response time characteristics have been improved to a few milliseconds by employing an overdrive method as well as controlling the alignment surface properties.

In our previous work, we reported nanoencapsulated LCDs with an IPS mode [16]. The droplets of nematic LCs within a nanoencapsulated LC layer have a size of about 300 nm, which is smaller than wavelength of visible light. Because the nanoencapsulated LC layer has optically isotropic properties, excellent electro-optical characteristics including the contrast ratio and viewing angle were realized. In addition, the nanoencapsulated LCD exhibited fast response time characteristics because the LCs were surrounded by the polymer shell with a strong anchoring energy. However, the high operating voltage was a burden on real display application.

In this study, we fabricated a nanoencapsulated LCD in IPS configuration with a polymer half-wall structure, which resulted in low driving voltage. In a conventional IPS LCD, electric fields are weaker around the top substrate because the electrodes are located only at the bottom substrate. The polymer half-walls located in the electrode region make it possible to enhance electric field strength between the interdigit electrodes. As a result, we could reduce the driving voltage by about 28%. Also, we developed a self-masking process for polymer walls and electrodes.

2. Experiments

We used a conventional coacervation method for LC nanoencapsulation [17]. A nematic host LC (HTW-106700, n_e = 1.745 and n_o = 1.504, Jiangsu Hecheng Display Technology Co.) was added to a mixture of nonionic polymer surfactants (polyethylene oxide–polypropylene oxide–polyethylene oxide block copolymers, Pluronic, BASF) and emulsifier (partially hydrolyzed polyvinyl alcohol, Aldrich) dissolved in an aqueous solution. The polymeric surfactant and emulsifier play important roles of reducing the surface tension and forming a shell material around the LC droplet, respectively. The resulting immiscible mixture was homogenized at room temperature using a magnetic stirring system, resulting in the formation of oil-in-water (O/W) nanoemulsions. Then, the mixture was heated up to the cloud point (about 50 °C) and kept at this temperature for several hours while being stirred, thereby allowing the PVA to become phase-separated around the nanoscale LC droplets and form a thin polymeric shell surrounding each droplet. The resulting nanoscale LC droplets encircled with thin polymeric membranes in the nanoemulsions were chemically crosslinked by the addition of crosslinking agents (glutaraldehyde, Sigma-Aldrich) to ensure that they were sufficiently strong to withstand external forces.

To fabricate the polymer wall structure, we developed a self-masking process. Figure 1 shows the schematic diagram of the fabrication process of the nanoencapsulated LCD. A positive-type photoresistor (PR) was spin coated on a glass substrate and baked on a hot plate at 100 °C for 10 min. The thickness was controlled by adjusting the spinning speed and was set to half of the cell gap. For the electrode, an aluminum (Al) layer was deposited on the PR

Optics EXPRESS

layer. Then, the second PR layer was coated on the Al layer. We exposed the structure to UV light through a photo-mask and developed the second PR layer. Because we used a positive-type PR, the UV-exposed area was removed. Then, the Al layer was patterned through a wet etching process. The width and the interval of the Al electrode were 10 μm and 15 μm, respectively. Next, the structure was exposed to UV again to fabricate the wall structure without any photo mask because the patterned Al layer acted as a self-photo mask. After developing the first PR layer, the PR wall structure could be formed with the IPS electrodes on top of the walls. To form the nanoencapsulated LC layer, we used a bar coater without any alignment layer or process. Next, a drying step was conducted so that the solvent was evaporated from the coated nanoencapsulated LC layer. Using a cover glass, we fabricated the IPS LC cell with a wall structure.

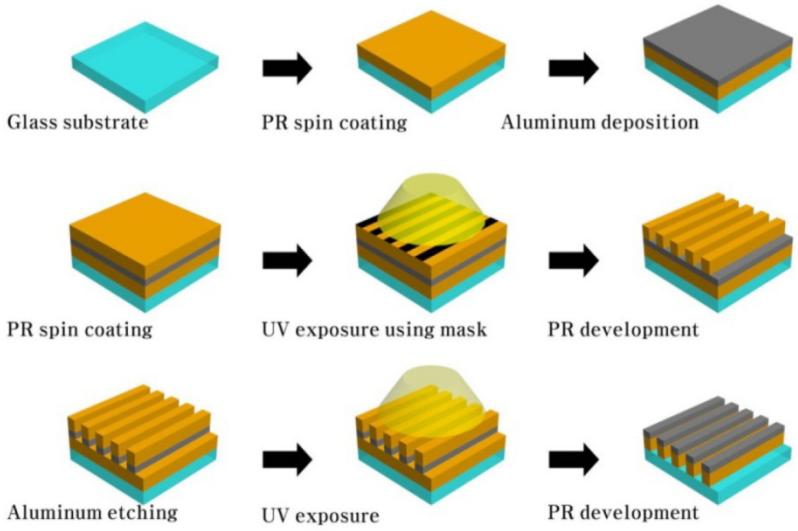

Fig. 1. Schematic diagram of the fabricated process.

3. Results and discussion

Figure 2(a) shows the typical particle size distribution of our LC nanocapsules obtained by the above-mentioned coacervation method. The mean diameter was about 200 nm, which is one third smaller than a wavelength of incident light (λ = 632 nm). Figure 2(b) shows a cross-sectional scanning electron microscope (SEM) image of our nanoencapsulated LCD with patterned electrodes onto the half-wall structure. The height of the wall was about 1.4 μm, which is a half of the nanoencapsulated LC layer thickness (~2.9 μm). The Al electrode was located on the top of the wall and in the center of the LC layer.

Figure 3 shows the voltage-transmittance and response time characteristics of the nanoencapsulated LC cell. The driving voltage for the nanoencapsulated LC cell with IPS electrodes on the substrate without the wall structure was 27.2 V while that for the nanoencapsulated LC cell with IPS electrodes on top of the wall structure (1.4 μm) was 19.5 V. By adopting the electrode on top of the half-wall structure, the driving voltage was significantly reduced. At 19.5 V, the total response time and contrast ratio was 2.2 ms and 2000:1, respectively.

To evaluate the effect of the location of the electrodes within the LC cell, we calculated the director of the LC molecules using a commercial simulator (TechWiz, Sanayi System, Korea). In the calculation, we assume nematic LC with very low elastic constants (0.1 pN) instead of nanocapsulated LCs since the encapsulated LC molecules were surrounded by polymer shell and the interaction between LC molecules in each droplet is very low. The

Optics EXPRESS

width of electrode and interval between electrodes are 10 μm and 15 μm, respectively. The cell gap was 3 μm.

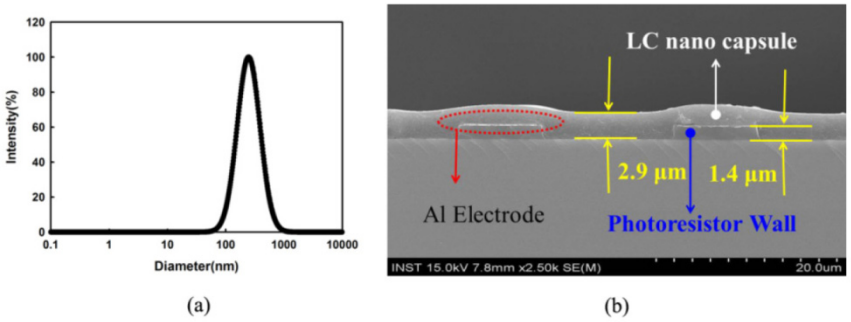

Fig. 2. (a) Particle size distribution of the LC nanocapsules prepared by coacervation method and (b) cross-sectional SEM image of the nanoencapsulated LC cell with the half-wall structure.

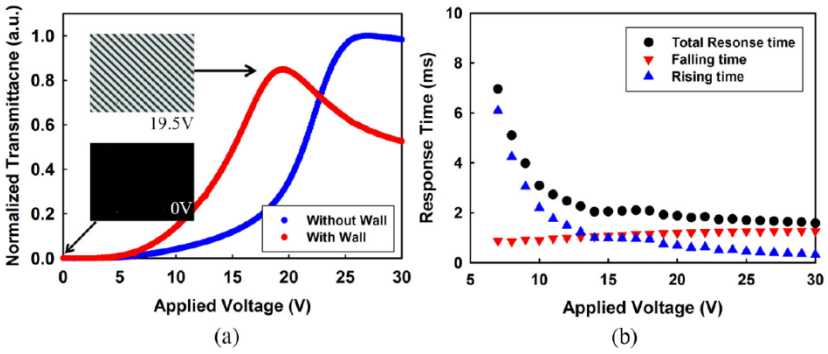

Fig. 3. (a) Voltage-transmittance characteristics of the nanocapsulated LC cells with/without a polymer wall (1.4 μm) and (b) response time characteristics of the nanocapsulated LC cell with the polymer half-wall. The inset boxes show the microscopic images under crossed polarizers for the cell with polymer half-wall.

In the conventional IPS cell, the electrodes are located on the bottom substrate. When we applied a voltage to the cell, the electric fields were weaker near the top substrate than around the bottom substrate. Namely, the lateral field strength which governs the optical anisotropy of the nanoencapsulated LC is significantly reduced along the direction of cell thickness. Therefore, the optical anisotropy of the LC droplets is not sufficiently switched as further away from the bottom substrate, as shown in Fig. 4(a). However, in our proposed structure, the electrodes are located in the middle of the LC layer. The distances from the electrodes to the top and bottom substrates are smaller than those in the conventional IPS cell. When we applied the same voltage as the conventional IPS cell, the optical anisotropy of the LC droplets was relatively uniform over the entire pixel regions, as shown in Fig. 4(b). Thus, the driving voltage could be reduced in our structure. However, the optical anisotropy of the LC droplets near the side of the wall did not sufficiently switch since the dielectric constant of the polymer wall is smaller than that of the nanoencapsulated LC layer (dashed regions in Fig. 4(b)). Therefore, the maximum transmittance of our proposed nanoencapsulated LC cell was reduced as shown in Fig. 3(a). We calculated the equipotential lines based on the simple electrostatics to verify an effect of the dielectric constant of the polymer wall on the potential distribution near the half-wall. Figures 4(c) and 4(d) show the equipotential lines near the electrode without/with wall structure, respectively. For calculation, the dielectric constant of the PR was assumed to be 4.2 which was smaller than the average dielectric constant of the

Optics EXPRESS

nanoencapsulated LC. As shown in Fig. 4(d), the lateral field strength was reduced but the vertical field strength was enhanced near polymer wall. It should be noted that the lateral field strength directly governs the optical anisotropy and the corresponding transmittance. Thus, the maximum transmittance in our cell would be reduced.

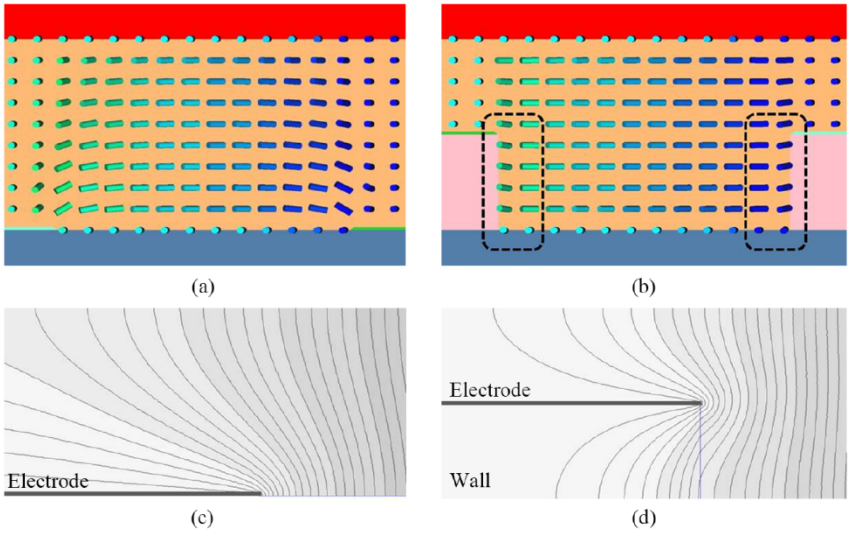

Fig. 4. LC director distributions of the LC cells (a) without and (b) with the wall structure, and equipotential lines (c) without and (d) with the wall structure in a simple electrostatic model.

Figure 5 shows the voltage-transmittance characteristics of the nanoencapsulated LC cells with/without the half-wall calculated from Fig. 4. Here, the relative voltage was scaled by the voltage exhibiting the maximum transmittance of the conventional IPS configuration. As mentioned above, the operating voltage with the maximum transmittance decreased in our proposed IPS configuration with the half-wall.

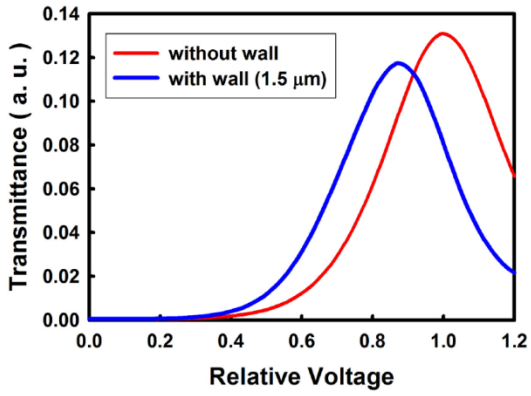

Fig. 5. Calculation results of the voltage-transmittance characteristics of the nanoencapsulated LC cells with/without the half-wall structure.

We also investigated an effect of the wall height on the operating voltage and the maximum transmittance. As shown in Fig. 6(a), the operating voltage with maximum transmittance was gradually decreased with increasing height of the wall. Noted that the operating voltage would be increased again after exceeding half of the thickness of the LC layer. The maximum transmittance was initially reduced by introducing the wall structure and increased until around 1.4 μm and again reduced as shown in Fig. 6(b). As mentioned in Fig.

Optics EXPRESS

4, the optical anisotropy of the LC droplets near the side of the wall did not sufficiently switch and thus transmittance would be reduced since the smaller dielectric constant of the polymer wall. However, the enhancement of the electric strength in the region upper wall electrode resulted in increase of the transmittance. Such competition gave rise to the variation of the maximum transmittance as shown in Fig. 6(b). In our experiment, the driving voltage decreased by 28%, and the transmittance decreased by 14% in the wall structure with 1.4 μm. If a wall material with higher dielectric constant than that of the encapsulated LC is used, the operating voltage is reduced but the maximum transmittance is not degraded.

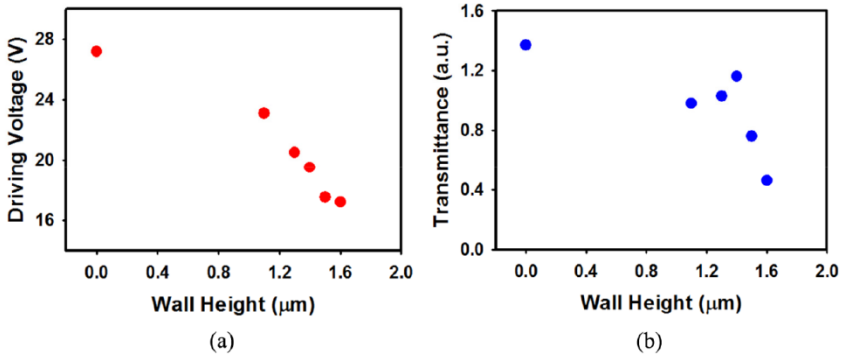

Fig. 6. (a) Operating voltage and (b) transmittance characteristics as functions of the height of the polymer wall.

4. Conclusion

We demonstrated the nanoencapsulated LCD with low operating voltage by introducing the half-wall structure with IPS electrodes on top of the half-wall. To reduce the operating voltage, the IPS electrodes were formed on top of the polymer wall by self-masking process. The polymer wall was fabricated by using the patterned IPS electrode on the positive-type PR layer as a photomask for photolithography. The height of the polymer wall was optimized at around half of the nanoencapsulated LC layer. Also, the maximum transmittance was investigated and discussed according to the height of the polymer wall.

Funding

This work was supported by the ICT R&D program of MSIP/IITP [10041416, The core technology development of light and space adaptable energy-saving I/O platform for future advertising service].